Identification of a miniature Sae2/Ctp1/CtIP ortholog from Paramecium tetraurelia required for sexual reproduction and DNA double-strand break repair

Julia Godau, Lorenza P. Ferretti, Anika Trenner, Emeline Dubois, Christine Von Aesch, Antoine Marmignon, Lauriane Simon, Aurélie Kapusta, Raphaël Guérois, Mireille Bétermier, et al.

Title: Identification of a miniature Sae2/Ctp1/CtIP ortholog from *Paramecium tetraurelia* required for sexual reproduction and DNA double-strand break repair

Authors: Julia Godau, Lorenza P. Ferretti, Anika Trenner, Emeline Dubois, Christine von Aesch, Antoine Marmignon, Lauriane Simon, Aurélie Kapusta, Raphaël Guérois, Mireille Bétermier, Alessandro A. Sartori

PII: S1568-7864(18)30259-3
DOI: https://doi.org/10.1016/j.dnarep.2019.03.011
Reference: DNAREP 2607

To appear in: *DNA Repair*

Received date: 13 October 2018
Revised date: 28 January 2019
Accepted date: 21 March 2019

Please cite this article as: Godau J, Ferretti LP, Trenner A, Dubois E, von Aesch C, Marmignon A, Simon L, Kapusta A, Guérois R, Bétermier M, Sartori AA, Identification of a miniature Sae2/Ctp1/CtIP ortholog from *Paramecium tetraurelia* required for sexual reproduction and DNA double-strand break repair, *DNA Repair* (2019), https://doi.org/10.1016/j.dnarep.2019.03.011

Identification of a miniature Sae2/Ctp1/CtIP ortholog from *Paramecium tetraurelia* required for sexual reproduction and DNA double-strand break repair

Short title: Minimal CtIP from *Paramecium* supports homologous recombination

Julia Godau[1¶], Lorenza P. Ferretti[1¶,#a], Anika Trenner[1], Emeline Dubois[2], Christine von Aesch[1], Antoine Marmignon[2], Lauriane Simon[2], Aurélie Kapusta[2,#b], Raphaël Guérois[2], Mireille Bétermier[2]* and Alessandro A. Sartori[1]*

[1]Institute of Molecular Cancer Research, University of Zurich, Zurich, Switzerland

[2]Institute for Integrative Biology of the Cell (I2BC), CEA, CNRS, Univ. Paris-Sud, Université Paris-Saclay, Gif-sur-Yvette, France

[#a]Current Address: Department of Molecular Mechanisms of Disease, University of Zurich, Zurich, Switzerland

[#b]Current Address: Department of Human Genetics, University of Utah School of Medicine, Salt Lake City, United States of America

*Corresponding authors

E-mails: sartori@imcr.uzh.ch (AAS), mireille.betermier@i2bc.paris-saclay.fr (MB)

[¶]These authors contributed equally to this work.

Highlights

- *Paramecium* CtIP constitutes the smallest known ortholog of the Sae2/CtIP family
- *Paramecium* CtIP is required for the repair of Spo11-induced breaks during meiosis
- CtIP proteins utilize a highly conserved RHR motif for DNA-binding
- The RHR motif of human CtIP supports its accumulation at damage chromatin
- Mutation of the human CtIP-RHR motif confers DSB resection and repair defects

Abstract

DNA double-strand breaks (DSBs) induced by genotoxic agents can cause cell death or contribute to chromosomal instability, a major driving force of cancer. By contrast, Spo11-

dependent DSBs formed during meiosis are aimed at generating genetic diversity. In eukaryotes, CtIP and the Mre11 nuclease complex are essential for accurate processing and repair of both unscheduled and programmed DSBs by homologous recombination (HR). Here, we applied bioinformatics and genetic analysis to identify *Paramecium tetraurelia* CtIP (PtCtIP), the smallest known Sae2/Ctp1/CtIP ortholog, as a key factor for the completion of meiosis and the recovery of viable sexual progeny. Using *in vitro* assays, we find that purified recombinant PtCtIP preferentially binds to double-stranded DNA substrates but does not contain intrinsic nuclease activity. Moreover, mutation of the evolutionarily conserved C-terminal 'RHR' motif abrogates DNA binding of PtCtIP but not its ability to functionally interact with Mre11. Translating our findings into mammalian cells, we provide evidence that disruption of the 'RHR' motif abrogates accumulation of human CtIP at sites of DSBs. Consequently, cells expressing the DNA binding mutant CtIP$^{R837A/R839A}$ are defective in DSB resection and HR. Collectively, our work highlights minimal structural requirements for CtIP protein family members to facilitate the processing of DSBs, thereby maintaining genome stability as well as enabling sexual reproduction.

Keywords

Paramecium tetraurelia; CtIP; Meiosis; DNA double-strand breaks; Homologous recombination; DNA end resection

1. Introduction

DNA double-strand breaks (DSBs) are the most lethal type of DNA damage, and, if incorrectly repaired, can drive tumorigenesis [1]. On the other hand, induction of DSBs by ionizing radiation (IR) or DNA topoisomerase poisons like camptothecin (CPT) represents a common therapeutic strategy to effectively eliminate cancer cells [2]. Cells have evolved two major pathways for the repair of DSBs: Non-homologous end-joining (NHEJ), which ligates broken ends without the need of extensive processing, and homologous recombination (HR), which requires an intact homologous DNA template for repair [3,4]. The first step of HR is termed DNA-end resection and involves nucleolytic processing of DSB ends to generate 3' single-stranded DNA (ssDNA) overhangs that are immediately covered by the replication protein A (RPA). RPA subsequently gets replaced by the Rad51 recombinase, which initiates homology search and strand invasion [5]. In eukaryotes, DNA-end resection is initiated by the concerted action of the Mre11-Rad50-Xrs2/Nbs1 (MRX/N) nuclease complex in association with Sae2/Ctp1/CtIP [5].

At the protein level, human CtIP and its counterparts in other species are predicted to be largely intrinsically disordered, with the exception of a conserved N-terminal coiled-coil domain that assembles into a tetrameric 'dimer-of-dimers' complex [6,7]. In addition, a short C-terminal stretch showing the highest degree of amino acid sequence similarity within CtIP protein members is commonly referred to as the 'Sae2-like' domain [8]. Human CtIP and its functional counterparts in *S. pombe* (Ctp1), *A. thaliana* and *C. elegans* have been identified as homologs of *S. cerevisiae* Sae2 (Sporulation in the absence of Spo eleven 2), a protein that is required for the initiation of DNA-end resection in meiotic and mitotic yeast cells [9-14].
The biochemical properties of recombinant Sae2/Ctp1/CtIP proteins have been extensively studied in recent years, significantly contributing to our mechanistic understanding of DNA-end resection [8]. First, both Sae2 and CtIP were shown to directly associate with the MRX and MRN complex, respectively, and to stimulate Mre11's weak endonuclease activity in cleaving the 5' strand [14-20]. In a second step, DNA is processed in 3' to 5' direction from the nick towards the DSB end by Mre11's intrinsic exonuclease activity, meanwhile 5' to 3' exonucleases such as Exo1 and Dna2 progressively resect the 5' DNA strand, ultimately generating a 3' single-stranded DNA (ssDNA) overhang compatible for Rad51 binding [21-24].

In the germline, the formation of programmed DSBs, generated by the topoisomerase-like Spo11 protein, is required for genetic recombination during meiosis [25]. Throughout evolution, CtIP and the Mre11 nuclease complex are strictly required for meiotic recombination by removing covalently attached Spo11 from DSB ends and, thereby, allowing DNA-end resection to start [26-30]. *Paramecium tetraurelia*, like all ciliates, is a unicellular eukaryote that contains two functionally distinct types of nuclei: a large somatic macronucleus (MAC, 800*n*) responsible for gene expression, but not transmitted to sexual progeny, and two identical diploid germline micronuclei (MIC) that undergo meiosis during the sexual cycle [31]. In *P. tetraurelia*, correct assembly of newly developing MACs requires the elimination of 25-30% of MIC DNA, including the precise excision of thousands of ~45,000 short internal eliminated sequences (IES) [31]. DNA elimination is mediated through the sequential action of PiggyMac, a domesticated piggyBac transposase essential for cleaving DNA at IES ends, and the NHEJ pathway [31-35]. With regards to recombinatorial repair, a recent inventory of meiosis-specific genes in ciliates revealed the presence of two gene copies each for *PtMRE11* and *PtCtIP*, consistent with multiple whole-genome duplication events in the early stages of *P. tetraurelia* evolution [36,37]. Remarkably, with a length of only 198 amino acids, PtCtIP paralogs would constitute the smallest

Sae2/Ctp1/CtIP protein family members that have been identified so far.

In the present study, we sought to characterize the function of PtCtIP *in vivo* and *in vitro*. Comparative sequence analysis reveals that PtCtIPa and PtCtIPb, collectively termed as PtCtIP, share the minimal domain architecture present in all Sae2/Ctp1/CtIP proteins. *PtCtIP* expression is required for the processing of Spo11-dependent meiotic DSBs, an essential prerequisite to the production of gametic nuclei and subsequent development of a new somatic MAC in sexual progeny. Purified recombinant PtCtIP binds with high affinity to double-stranded branched DNA molecules but lacks detectable intrinsic nuclease activity. Moreover, PtCtIP-DNA interaction, but not PtCtIP-Mre11 interaction, strongly depends on a highly conserved 'RHR' motif located in the C-terminus. Finally, we provide evidence that the 'RHR' motif mediates efficient recruitment of human CtIP to sites of DNA damage ensuring efficient DSB resection and repair by HR.

2. Results

2.1. Paramecium tetraurelia encodes two protein copies with a domain organization shared by CtIP homologs

CtIP protein sequences are poorly conserved across the eukaryote phylogeny and vary greatly in their molecular size, particularly between yeast and mammalian homologs (Fig. 1A). *Schizosaccharomyces pombe* Ctp1 (294 amino acids, aa) represents the smallest CtIP homolog that has been characterized so far [11]. To screen for additional members of the Sae2/Ctp1/CtIP protein family in other species, we ran iterative PSI-BLAST searches using as query the amino acid sequence of the conserved C-terminal domain of human CtIP (~75 aa). Interestingly, we retrieved two putative CtIP-like polypeptides in *Paramecium tetraurelia* comprised of only 198 aa sharing more than 80% sequence identity (Fig. 1A and Supplemental Fig. 1A). Closer examination of the *P. tetraurelia* predicted proteome indeed revealed the existence of two closely related CtIP paralogs, PtCtIPa and PtCtIPb (ParameciumDB accession numbers GSPATP00020534001 and GSPATP00027328001) [38]. *PtCtIPa* and *PtCtIPb* gene copies resulted from the most recent whole genome duplication (WGD) that took place before the evolutionary split of the *Paramecium aurelia* genus into 15 sibling species including *P. tetraurelia* [37].

To gain further insight into the protein sequence and domain architecture of PtCtIP, we adopted a hierarchical alignment procedure allowing us to align different evolutionarily conserved regions of CtIP homologs. The N-terminus of PtCtIP features five repeating heptad

sequences, which are predicted to assemble into a coiled-coil structure typically present in Sae2/Ctp1/CtIP proteins (Fig. 1A and Supplemental Fig. 1B). Moreover, upstream of the heptad repeats, a short α-helical region previously reported to mediate CtIP tetramerization can be distinguished with high confidence in PtCtIP (Supplemental Fig. 1B) [6,7]. The phylogenetic tree built from a multiple sequence alignment restricted to the conserved C-terminal domain demonstrates that PtCtIP clusters together with protozoan sequences, as expected, while strong sequence divergences are primarily observed between ascomycetes, including *S. cerevisiae* Sae2 (Fig. 1B and C). Closer examination of the PtCtIP C-terminal region revealed the presence of two conserved, closely spaced, short linear sequence motifs: 'CxxC' and 'RHR' (Fig. 1C). The 'RHR' motif, located at aa positions 181-183 of PtCtIP, was shown to promote DNA-bridging activity of Ctp1 *in vitro* [8]. We further noted that PtCtIP is the only family member lacking a C-terminal amino-acid extension after the cyclin-dependent kinase (CDK) consensus sequence motif (S/TP) required for DNA-end resection in yeast and human cells (Fig. 1C) [39,40]. In fact, PtCtIP lacks any additional CDK phosphorylation sites reported to promote the interaction of human CtIP with Nbs1 FHA/BRCT domains [41], suggesting that it is not prone to be regulated in a cell-cycle regulated manner but rather at the level of transcription. Consistent with this observation, no apparent homolog of Nbs1 exists in *P. tetraurelia*. In conclusion, our *in silico* analysis predicts that PtCtIP is mainly composed of the conserved N- and C-terminal regions of the Sae2/Ctp1/CtIP family, making it the smallest CtIP ortholog known to date.

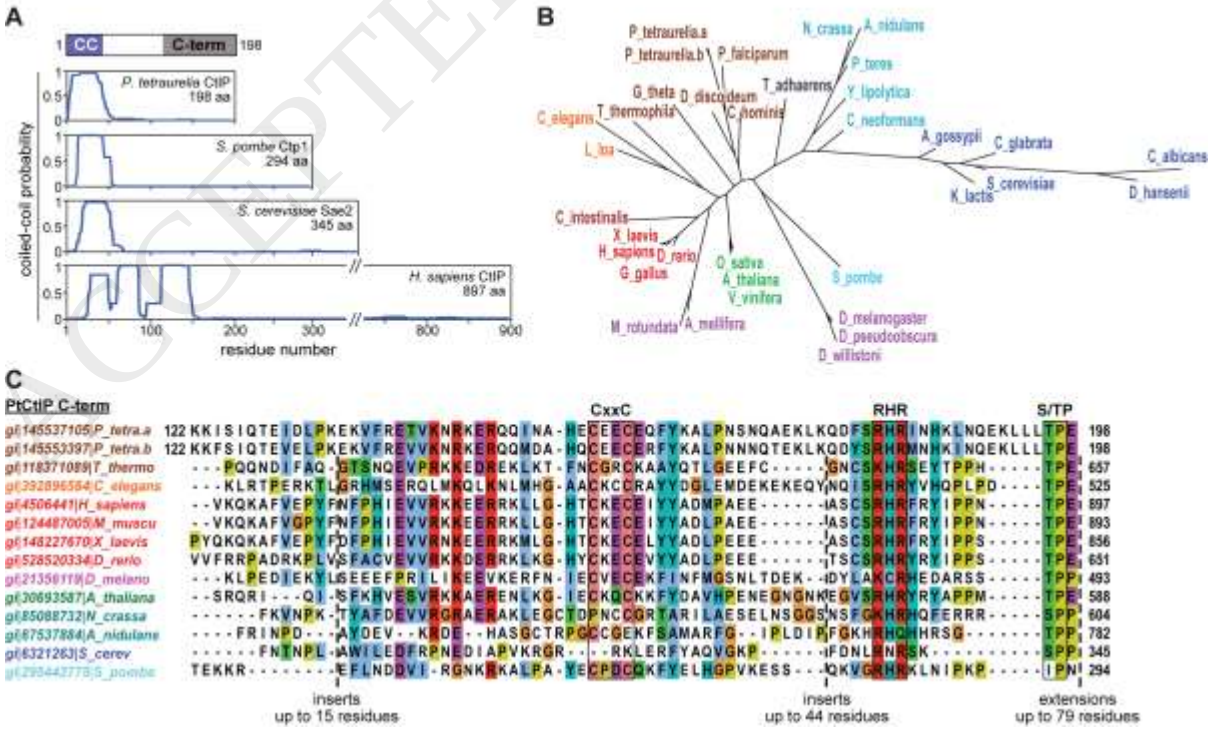

Fig. 1: Comparative protein sequence analysis of PtCtIP. (A) Upper panel, predicted protein scheme of *Paramecium tetraurelia* CtIP (PtCtIP) with putative coiled-coil (CC) and C-terminal regions indicated in coloured boxes. Lower panel, coiled-coil-forming probabilities predicted by the PCOILS program (window length of 21 residues) for the indicated CtIP proteins. **(B)** Phylogenetic tree obtained from the sequence analysis of the CtIP C-terminal region from 35 species using PhyML algorithm. **(C)** Sequence alignment of the C-terminal region of PtCtIPa and PtCtIPb with 12 CtIP proteins from different species. Gene accession numbers (gi) and species names are color-coded according to the phylogenetic tree shown in **(B)**. Insertions and extensions were trimmed and marked by dashed lines with the number of residues indicated below. Evolutionarily conserved CxxC, RHR and S/TP motifs are indicated in black boxes.

2.2. Paramecium CtIP genes are required for the recovery of viable progeny during autogamy

Autogamy is a self-fertilization process encountered in the *Paramecium aurelia* group of species (Supplemental Fig. 2A). Upon starvation, mature *P. tetraurelia* cells that have undergone at least 20 vegetative fissions can start MIC meiosis in the absence of a sexual partner. A fully homozygous zygotic nucleus is formed through the fusion of two identical gametic nuclei. Following two successive nuclear divisions that take place in the absence of cell division, two mitotic copies of the zygotic nucleus give rise to the new MICs while new MACs differentiate from the other two copies. We surveyed the expression of *PtCtIP* compared to *PtSPO11* in *P. tetraurelia* cells at different autogamy stages. Northern blot analysis revealed an early transcription induction peak during MIC meiosis for both *PtCtIP* genes simultaneously to *PtSPO11* (Supplemental Fig. 2B). This result was confirmed by deep sequencing of mRNAs (Fig. 2A) [42]. As expected from the conservation of the meiosis process in *Paramecium*, the genome of *P. tetraurelia* carries two recently duplicated *PtMRE11* genes. Northern blot hybridization and deep sequencing of mRNAs revealed that *PtMRE11* genes have quite different patterns of expression: *PtMRE11a* (ParameciumDB accession number GSPATG00020413001) exhibits a constitutively low level of expression at all stages of the sexual cycle, while *PtMRE11b* (ParameciumDB accession number GSPATG00023641001) is strongly induced during meiosis (Fig. 2A and Supplemental Fig. 2B) [38]. Notably, *PtMRE11b* levels peak at the same time during meiosis as both *PtCtIP* and *PtSPO11* mRNAs (Fig. 2A and Supplemental Fig. 2B).

To gain insight into the function of CtIP in *P. tetraurelia*, we used an RNAi strategy to silence the expression of *PtCtIP* genes during autogamy, individually or altogether. Because both genes are actively transcribed during meiosis (Fig. 2A and Supplemental Fig. 2B), vegetative growing cells were fed on dsRNA-producing bacteria and left to starve in the feeding medium until autogamy started. Quantitative analysis of mRNA levels using northern blot hybridization demonstrated an efficient RNAi-mediated downregulation of *PtCtIPa* and *b* (up to ~10 fold) relative to control RNAi (Fig. 2B and Supplemental Fig. 2C). During

autogamy of cells silenced for the expression of both *PtCtIPa* and *b* genes, the development of new MACs in the sexual progeny was monitored after DAPI staining. Strikingly, in all *PtCtIP* knockdowns, a large fraction of autogamous cells harboured only fragments from the old MAC, but did not develop new MACs (Supplemental Fig. 2C and D). No MICs could be detected in these cells either, suggesting that depletion of PtCtIP triggers an early defect during the sexual cycle and prevents the formation of a functional zygotic nucleus. At later stages, cells with two MICs and a single large nucleus surrounded by several smaller fragments started to appear in *PtCtIP* knockdowns (orange population in Supplemental Fig. 2C). These could result from the overgrowth of a minority of viable post-autogamous progeny that succeeded in making their new MACs, throughout the long incubation time of each experiment (3 to 4 days).

To check whether knockdown of *PtCtIP* or *PtMRE11* genes has a debilitating effect on the ability of sexual progeny to resume vegetative growth, we measured the percentage of post-autogamous survivors with functional new MACs. Knockdown of individual *PtCtIPa* or *b* genes did not cause any reduction of viable progeny, suggesting that *PtCtIP* genes can compensate each other (Fig. 2C). However, the concomitant inactivation of both *PtCtIPa* and *b* expression resulted in ~70% lethality in sexual progeny (Fig. 2C). In contrast, silencing of *PtSPO11* or *PtMRE11b* alone was sufficient to induce strong lethality in post-autogamous progeny, consistent with their respective meiosis-specific expression profiles (Fig. 2A and Supplemental Fig. 2B). These results indicate that, despite its short size, PtCtIP, like PtMre11, is fully functional and essential for DSB repair during meiosis in *P. tetraurelia*.

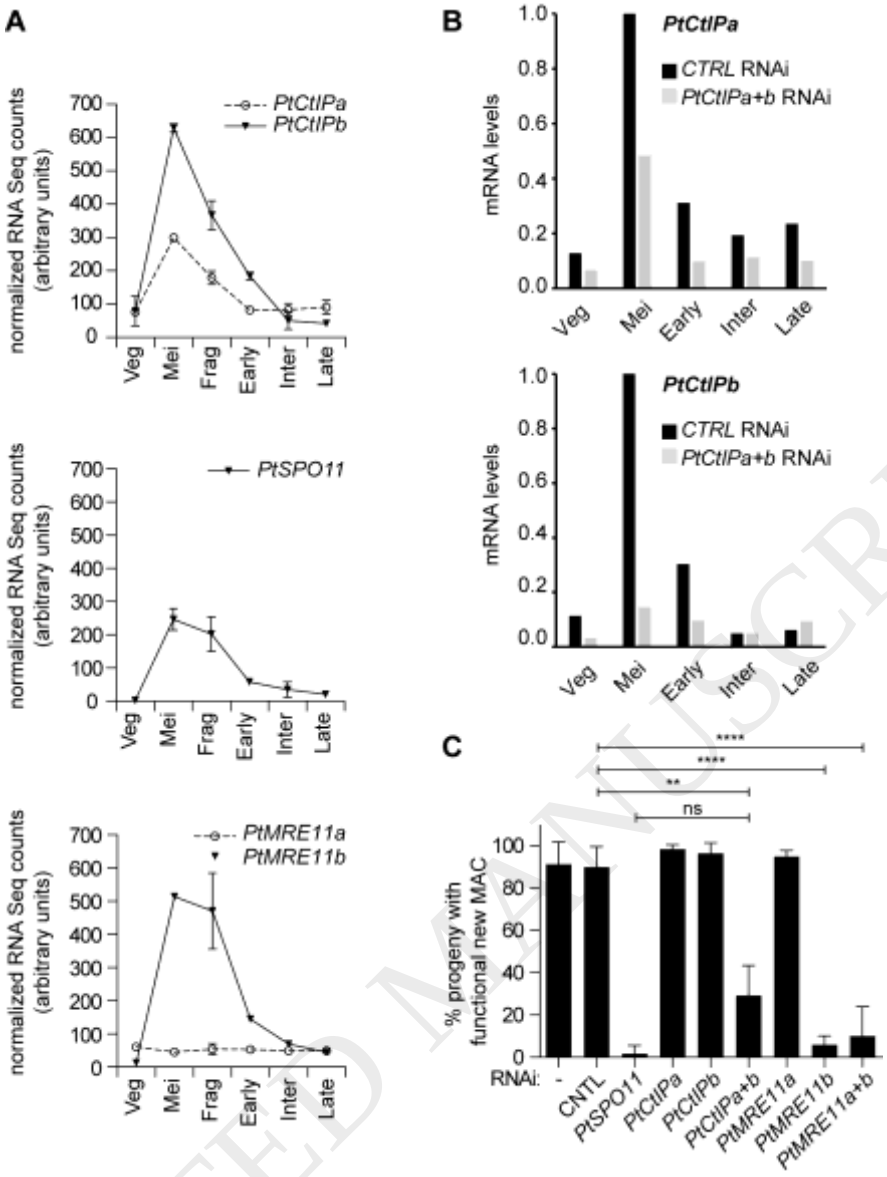

Fig. 2: *PtCtIP* genes are required for recovery of viable sexual progeny. (A) Steady-state levels for *PtCtIP*, *PtSPO11* and *PtMRE11* mRNA at different developmental stages. Curves show the average normalized values calculated for each autogamy stage (n ≥ 2). RNA-Seq data extracted from [42]. Veg: vegetative cells; Mei: starved cells with meiotic stages; Frag: fragmented old MAC but no visible developing new MACs; Early: early stages of MAC development; Inter: intermediate stages of MAC development; Late: late stages of MAC development. **(B)** Quantification of *PtCtIPa* and *PtCtIPb* mRNA levels during autogamy. *P. tetraurelia* 51 cells were subjected to control RNAi (*ND7*) or RNAi against both *PtCtIPa* and *PtCtIPb* (*PtCtIPa+b*). Autogamy stages were defined as in (A) following DAPI staining of nuclei. Northern blots of total RNAs extracted at indicated time-points for each RNAi condition were hybridized with *PtCtIPa*- or *PtCtIPb*-specific labeled probes A2 (upper panel) or B2 (lower panel), respectively (Supplemental Fig. 2C and Supplemental Table S1). Viable post-autogamous progeny yields in this experiment: 97%, control RNAi; 23%, *PtCtIPa+b* RNAi. 17S rRNA signal was used for normalization. Y-axes are in arbitrary units, with CTRL mRNA signals normalized to 1 at the Mei stage for each probe. **(C)** Combined depletion of *PtCtIPa* and *PtCtIPb* impairs new MAC development in *Paramecium* sexual progeny. Histograms show the fraction of sexual progeny harboring functional new MACs after silencing of the respective genes by RNAi. Data are presented as the mean ± SD with n between 2 and 15 for each condition. Statistical differences were determined by paired t-test. ns, non-significant; ** ($P < 0.005$); **** ($P < 0.0001$). CNTL: RNAi-mediated targeting of either *ND7* or *ICL7* non-essential genes. For simultaneous silencing of both *PtMRE11* genes, different constructs were used (cross-reacting a2 and b2 constructs, either alone or together; gene-specific a1 and b1 constructs, together; see Supplemental Table S1).

2.3. Abnormal meiosis and lack of new developing MACs in cells depleted for PtCtIP genes

The complete absence of new MICs and MACs in *PtCtIP* knockdowns likely reflects an early defect in the formation of a functional zygotic nucleus. In the ciliate *T. thermophila*, *SAE2/COM1* knockout was shown to block the progression of MIC meiosis at the meiosis I stage, as a result of defective repair of meiotic DSBs and inefficient pairing of homologous chromosomes, eventually leading to chromosome "disintegration" and MIC degeneration [43]. Because autogamy is poorly synchronous in *P. tetraurelia*, we switched to conjugation in order to synchronize MIC meiosis and zygotic nucleus formation in the population [44]. We used anti-γ-tubulin antibodies to specifically label the MICs, the zygotic nucleus and its mitotic division products [45] in conjugating cells co-silenced for both *PtCtIP* genes (Fig. 3A and Supplemental Fig. 3). This experiment confirmed that MIC meiosis proceeded normally at the cytological level, until the 4-MIC stage (*i.e.* meiosis I) in a large majority of cells. Abnormal patterns started to appear at meiosis II, with partial or complete loss of MIC meiotic products and complete absence of a zygotic nucleus in a majority of mating pairs, while normal fragmentation of the old MAC was still observed, suggesting that no fragmentation checkpoint exists in *P. tetraurelia*. Therefore, CtIP depletion in *P. tetraurelia* does not allow the formation of a zygotic nucleus, because it triggers an arrest right after meiosis I.

In other organisms, the absence of CtIP also results in abortive meiosis, due to the accumulation of unrepaired Spo11-dependent DSBs. In *S. pombe*, *ctp1* C-terminal mutations severely reduce the yield of viable spores [27]. In budding yeast, *sae2*Δ mutant cells do not form tetrads, but sporulation is restored in the *sae2*Δ*spo11*Δ double mutant background, even though the resulting spores are not viable [12,13]. To get further insight into the meiotic function of the *P. tetraurelia* CtIP homologs, we knocked down *PtSPO11* by inducing a Δ*SPO11* somatic deletion (Δ$SPO11_{MAC}$) in strain 51 new (see Methods). We then submitted wild-type and Δ$SPO11_{MAC}$ cells to RNAi against *PtCtIP* genes and to a control RNAi against *ND7*. As expected, Δ$SPO11_{MAC}$ cells did not yield viable progeny in either condition (*PtCtIP* or control RNAi, Supplemental Fig. 4A). During the progression of autogamy, significant differences were observed between Δ$SPO11_{MAC}$ and wild-type cells (Fig. 3B). In wild-type cells, *PtCtIP* silencing strongly impaired the formation of developing new MACs, as already observed. In the Δ$SPO11_{MAC}$ mutant submitted to a control RNAi, new developing MACs were detected, although not quite with the same efficiency as in the wild-type background. However, as indicated by the low survival rate in the progeny of Δ$SPO11_{MAC}$ cells (Supplemental Fig. 4A), these new MACs were not functional, suggesting that in *P.*

tetraurelia, similar to other organisms, Spo11-dependent DSBs are essential for the successful segregation of homologs during meiosis. A dramatic difference was observed between wild-type and Δ*SPO11*$_{MAC}$ cells upon the silencing of *PtCtIP*. Indeed, the development of new MACs, strongly impaired in a *PtCtIP* knockdown, was partially restored in the double *PtSPO11* + *PtCtIP* knockdown, indicative of a role for the *Paramecium* CtIP homologs in the repair of Spo11-dependent meiotic DSBs. Likewise, a double RNAi experiment revealed that MAC development is restored following *PtMRE11b* RNAi if cells are simultaneously submitted to RNAi against *PtSPO11* (Supplemental Fig. 4B and C). Taken together, these results demonstrate a key function of PtCtIPa+b and PtMRE11b in repairing Spo11-induced DSBs during meiosis and indicate that PtCtIP, despite its short size, is fully functional for promoting HR in *P. tetraurelia*.

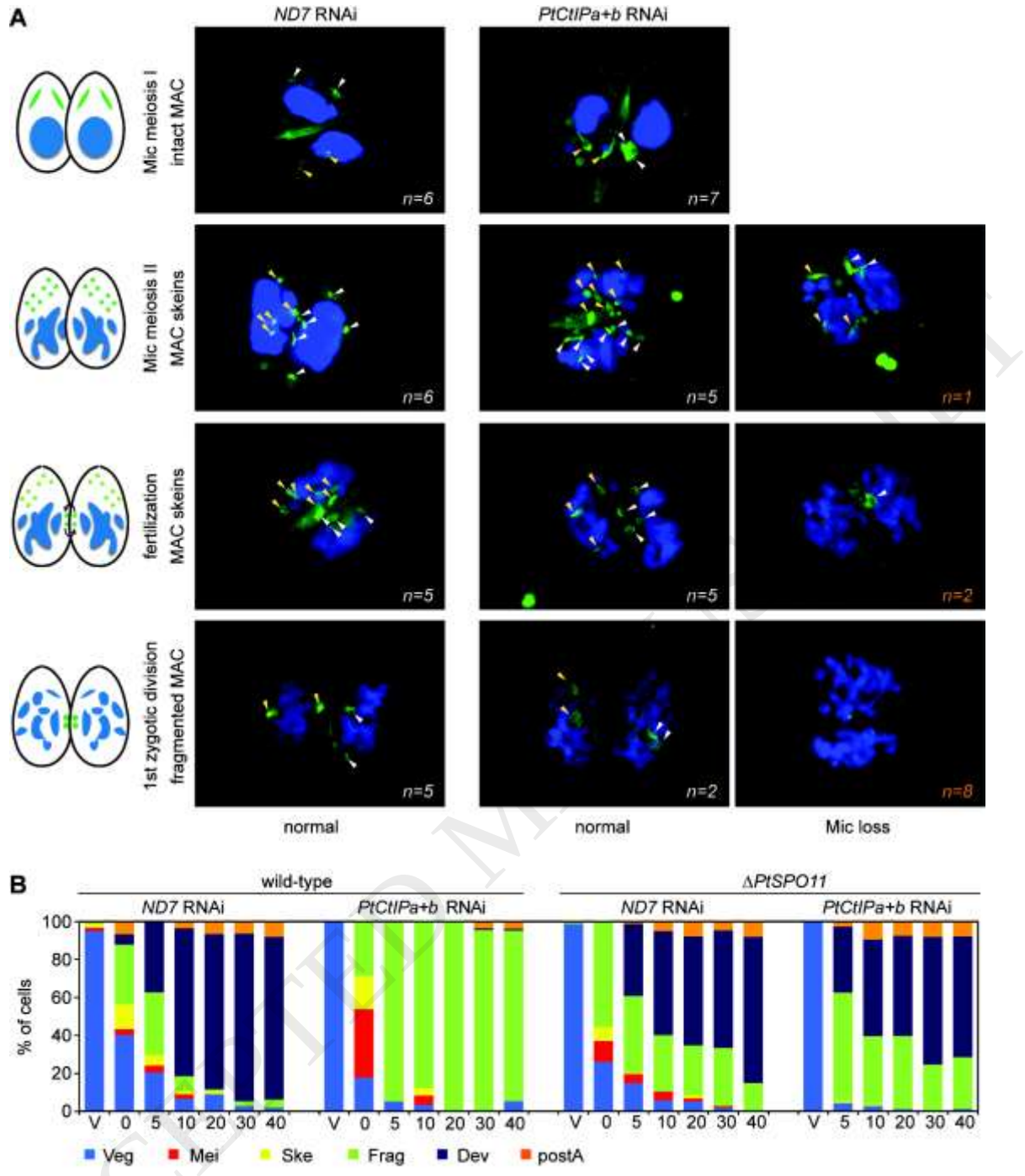

Fig. 3: *PtCtIP* silencing impairs new MAC development due to abortive meiosis. (A) *PtCtIP* RNAi during conjugation triggers a meiotic defect and impairs zygotic nucleus formation. Reactive cells prepared in control (*ND7*) or *PtCtIPa+b* RNAi medium were crossed at T0 and mating pairs were permeabilized and fixed 4.5, 6 and 7.5 hours following the start of conjugation. Fixed cells were pooled before proceeding to immunofluorescence staining using anti-γ-tubulin antibodies (green) and DAPI staining of nuclei (separate channels of the same images are shown in Supplemental Fig. 3). The progression of conjugation was monitored according to the state of the old MAC. Arrowheads (yellow in one partner, white in the other) point to meiotic micronuclei, or to zygotic nuclei and their mitotic products. 22 and 30 mating pairs were analyzed for the control (*ND7*) and for *PtCtIP* RNAi, respectively. Numbers in orange refer to pairs in which loss of micronuclei ('Mic loss') was detected in one or both partners. In the experiment shown here, 37% of mating pairs yielded viable progeny in the *PtCtIP* RNAi (100% in the control RNAi). **(B)** MAC development is inhibited following *PtCtIPa+b* RNAi in wild-type cells and restored at the cytological level in a *SPO11* knockout *Paramecium* strain submitted to *PtCtIPa+b* RNAi. Cultures of isogenic wild-type and Δ*PtSPO11* cells were allowed to undergo autogamy in control (*ND7*) or *PtCtIP* RNAi-inducing medium. The histograms show the progression of autogamy in the four cultures, as monitored by DAPI staining of cells at indicated time-points (hours), with the

different cellular stages indicated below. Veg: vegetative cells; Mei: meiotic cells; Ske: cells with MAC skeins; Frag: cells with old MAC fragments but no visible new developing MACs; Dev: cells with two developing MACs; postA: post-autogamous cells with one new MAC and remaining old MAC fragments. Viable post-autogamous progeny yields in this experiment: 93%, wild-type cells, control RNAi; 10%, wild-type cells, *PtCtIP* RNAi, 7%, *ΔPtSPO11* cells, control RNAi; 0% *ΔPtSPO11* cells, *PtCtIP* RNAi (see Supplemental Fig. 4A).

2.4. PtCtIP DNA-binding depends on a conserved C-terminal RHR motif

Our genetic analyses underscored an essential role for *CtIP* during autogamy and conjugation in *P. tetraurelia*. In order to investigate how PtCtIP contributes to DNA-end resection at the molecular level, we purified full-length recombinant PtCtIPa protein from insect cells (Supplemental Fig. 5A and B). First, we aimed to characterize its DNA-binding properties by *in vitro* gel shift assays using 5'-end radiolabeled 50-mer oligonucleotide substrates (Supplemental Table S1). At a fixed protein/DNA molar ratio, we observed that PtCtIPa specifically interacts with double-stranded, but not single-stranded nucleic acids (Fig. 4A). Further protein titration and DNA competition experiments revealed that PtCtIPa exhibits a slight binding preference for forked *versus* blunt-ended DNA (Fig. 4B and Supplemental Fig. 5C). We noted that PtCtIPa-DNA complexes migrated near the top of the gel, indicative of the formation of rather large multimeric assemblies, in particular when considering the low molecular weight of *Paramecium* CtIP (Fig. 4A and B). Interestingly, however, recent studies demonstrated that both Ctp1 and human CtIP N-terminal domains can form stable tetramers consisting of two coiled-coil dimers [6,7]. Thus, given that both structural motifs mediating Ctp1/CtIP tetramerization are conserved in PtCtIP (Supplemental Fig. 1B), it is conceivable to predict that recombinant PtCtIPa also exists as a tetramer in solution resulting in the formation of high molecular weight complexes upon DNA binding. Indeed, size exclusion chromatography analysis indicated a dominant oligomeric state for PtCtIPa and MBP-PtCtIPa, the latter of which eluting at similar retention volumes as Ctp1 (Supplemental Fig. 5D). Moreover, residual amounts of uncleaved MBP-PtCtIPa (67 kDa) fusion protein present in our preparations (Supplemental Fig. 5B) might explain why the DNA mobility shift is even slightly bigger compared with Ctp1 (Fig. 4B).

In addition to the N-terminal multimerization domain, Andres *et al.* reported a 'RHR' DNA-interaction motif located at the Ctp1 C-terminus [7]. As the 'RHR' motif is evolutionarily highly conserved among CtIP homologs from different species including *P. tetraurelia* (Fig. 1C), we expressed and purified recombinant PtCtIPa-AHA with R181 and R183 mutated to alanine residues (Fig. 4C and Supplemental Fig. 5B). Gel shift assays showed that the PtCtIP-AHA mutant was completely defective in binding to the forked-DNA

substrate, confirming the C-terminal 'RHR' motif as a critical determinant of DNA-binding by CtIP proteins (Fig. 4D). Notably, employing the same radiolabeled forked-DNA substrates, we could not detect any DNA cleavage activity associated with recombinant PtCtIPa (Supplemental Fig. 6A and B).

Remarkably, MBP-pulldown assays revealed that both wild-type (wt) PtCtIPa and the PtCtIP-AHA mutant are able to interact with recombinant human Mre11-Rad50 (MR) complex, suggesting an evolutionarily conserved mode of interaction between the two factors (Supplemental Fig. 6C). Human CtIP was shown to stimulate Mre11 endonuclease activity *in vitro* using different DNA substrates [14,18]. For instance, using closed-circular single-stranded PhiX174 DNA as a substrate, human CtIP specifically triggered robust MR-dependent endonucleolytic cleavage in the presence of magnesium but only mildly stimulated MR in the presence of manganese [14]. Under the exact same assay conditions as described therein, we observed that PtCtIPa is enhancing MR-mediated cleavage of PhiX174 DNA to a similar extent as human CtIP (Supplemental Fig. 6D and E). Interestingly, we could not reveal any difference in the amount of DNA cleavage products between PtCtIPa-wt and PtCtIP-AHA mutant, indicating that PtCtIP's DNA binding ability is largely dispensable for functionally interacting with MR *in vitro*. Taken together, our combined genetic and biochemical analysis of PtCtIP strongly supports its key role in DSB repair-related processes.

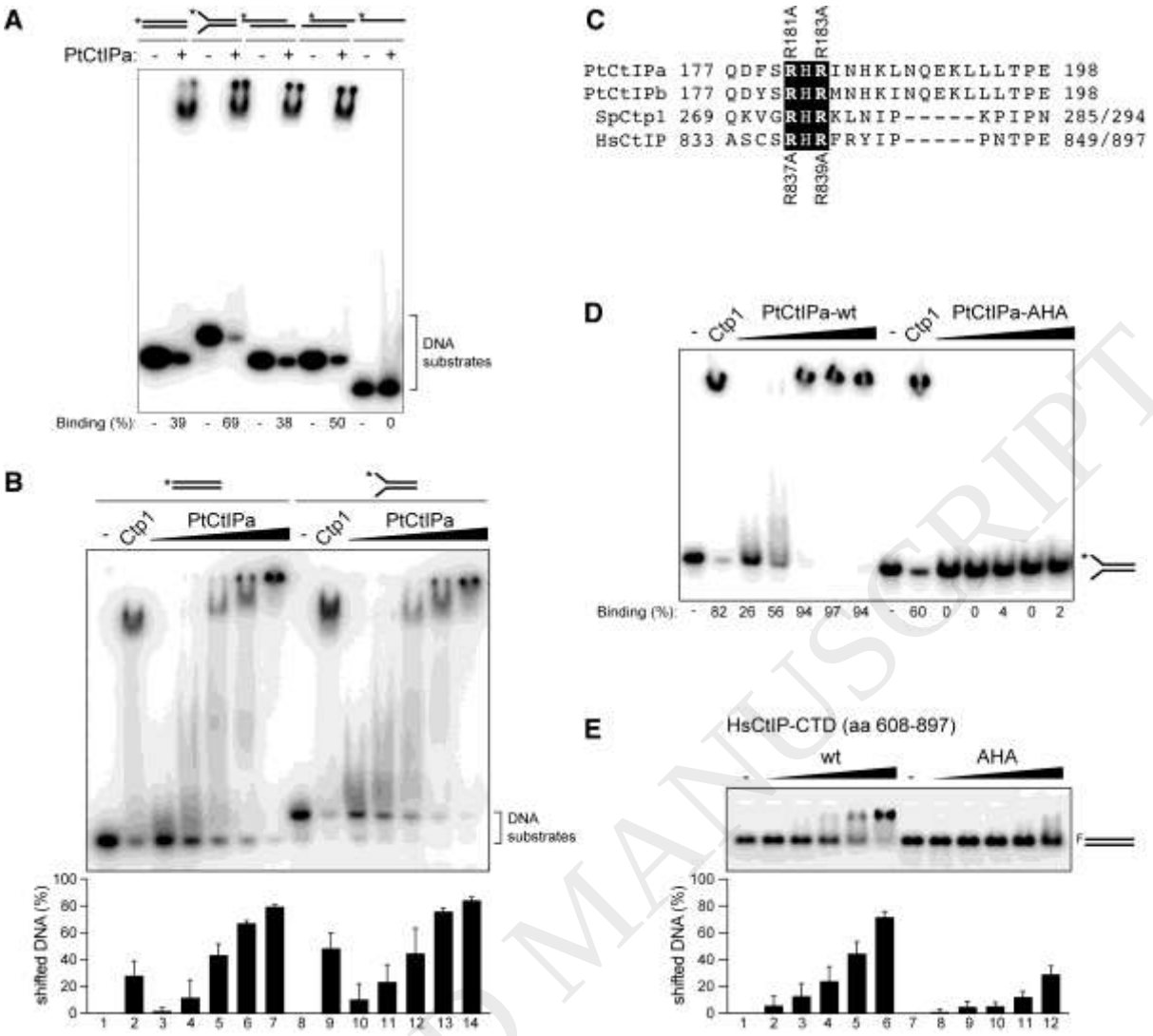

Fig. 4: PtCtIP and human CtIP require a highly conserved 'RHR' motif for DNA-binding. (A) PtCtIP binds double-stranded (ds) DNA. Electrophoretic mobility shift assay (EMSA) was carried out with 10 nM of various 5'-radiolabeled DNA substrates and 600 nM of PtCtIPa. Percentages of DNA binding were calculated based on the disappearance of the substrate band. **(B)** PtCtIP has a slight preference for forked DNA. Upper panel, EMSA was carried out with 10 nM of the indicated 5'-radiolabeled DNA substrates and increasing concentrations of PtCtIPa (100 nM, 200 nM, 400 nM, 700 nM and 1 µM). Ctp1 (380 nM) was used as a positive control. Lower panel, Percentages of DNA binding were calculated based on the disappearance of the substrate band. Data are represented as the mean ± SD (n = 3). **(C)** Alignment of the amino acid sequences adjoining the conserved RHR motif in CtIP homologs from *P. tetraurelia* (Pt), *S. pombe* (Sp) and *H. sapiens* (Hs). The R181A/R183A and R837A/R839A (AHA) mutations in PtCtIP and HsCtIP are indicated above and below the alignment, respectively. **(D)** Mutation of the RHR motif in PtCtIP abolishes DNA binding. EMSA was carried out with 10 nM of 5'-radiolabeled forked DNA substrates and increasing concentrations of PtCtIPa wild-type (wt) or AHA mutant (200 nM, 400 nM, 600 nM, 800 nM and 1 µM). Ctp1 (380 nM) was used as positive control. Percentages of DNA binding were calculated based on the disappearance of the substrate band. **(E)** Mutation of the RHR motif in human CtIP impairs binding to dsDNA. Upper panel, EMSA was carried out with 1 µM fluorescein (F)-labeled, blunt-ended dsDNA in presence of increasing concentrations of recombinant human CtIP C-terminal domain (CTD; 1 µM, 5 µM, 10 µM, 20 µM, 50 µM)). Lower panel, Percentages of shifted DNA in each lane were calculated by quantifying the fluorescence intensity of shifted relative to total DNA. Data are represented as the mean ± SD (n = 3).

2.5. Disrupting DNA-binding in human CtIP impairs DNA-end resection and HR

Consistently, we find that mutating the 'RHR' motif in human CtIP significantly reduced DNA binding activity of a recombinant C-terminal CtIP fragment purified from bacterial cells (Fig. 4C and E and Supplemental Fig. 7A and B). Williams and coworkers demonstrated that *S. pombe* strains expressing Ctp1 'RHR' mutant versions exhibited intermediate sensitivity to various genotoxic agents and failed to reconstitute full-length chromosomes following IR treatment, indicating a DSB repair defect [7]. However, the relevance of CtIP's DNA-binding ability to DNA-end resection and HR in human cells has so far not been investigated.

To determine whether disruption of the RHR motif in human CtIP confers cellular phenotypes in response to DNA damage, we generated stable U2OS Flp-In T-REx clones expressing doxycycline (Dox)-inducible siRNA-resistant GFP-tagged wild-type (wt) CtIP or a DNA binding-defective CtIP-AHA mutant (R837A/R839A). Importantly, flow cytometry and immunofluorescence microscopy analysis revealed that the two cell lines display similar cell cycle profiles and GFP-CtIP nuclear localisation patterns (Supplemental Fig. 8A and B). Moreover, CtIP-AHA mutant was efficiently phosphorylated at its nearby cyclin-dependent kinase (CDK) site (T847) critical for DNA-end resection [40], suggesting that DNA binding is not a prerequisite for regulatory CtIP modifications (Supplemental Fig. 8C). Given that recombinant PtCtIP-AHA was defective in DNA binding, we first examined the assembly of GFP-CtIP at DNA lesions induced by laser micro-irradiation. Importantly, previous studies have shown that Sae2/CtIP and Mre11 are independently recruited to sites of DSBs [46-48]. Remarkably, we observed that the GFP-CtIP fluorescent intensity at DSB-containing tracks marked with γH2AX was significantly reduced in the AHA mutant compared with the wt, suggesting that DNA binding is a critical determinant for CtIP retention at damaged chromatin (Fig. 5A and Supplemental Fig. 8D). CtIP is required for CPT-induced hyperphosphorylation of RPA2 at serines 4/8, a surrogate marker for DSB resection revealed by western blotting (Fig. 5B, lanes 1-3) [14,49]. We observed that re-expression of CtIP-wt fully restored RPA2 hyperphosphorylation in CtIP-depleted cells, whereas the rescue with CtIP-AHA was only partial (Fig. 5B, lane 7). Of note, GFP-CtIP expression as well as ATM phosphorylation levels were comparable between the two cell lines, indicating proficient upstream DSB signalling (Fig. 5B). Consistently, using a flow cytometry-based approach to measure DNA-end resection [50,51], we found that RPA retention on damaged chromatin is strongly reduced in AHA mutant compared to wt expressing cells (Fig. 5C). To further evaluate the impact of CtIP DNA binding on the processing of replication-associated DSBs formed at collapsed replication forks, we depleted endogenous CtIP from our U2OS clones

and measured their viability following chronic exposure to CPT. In agreement with previous data [51], activation of CtIP-wt expression by Dox administration efficiently rescued CPT hypersensitivity of CtIP-depleted cells (Fig. 5D). By contrast, cells expressing the CtIP-AHA mutant remained sensitive to CPT, indicative of an HR defect (Fig. 5D). Finally, to directly measure HR efficiency, we made use of the traffic-light reporter (TLR) assay system [6] and engineered U2OS-TLR clones stably expressing siRNA-resistant FLAG-tagged CtIP-wt and -AHA (Fig. 5E). Strikingly, whereas HR and DNA-end resection were largely restored in CtIP-depleted cells complemented with CtIP-wt, they were still significantly compromised in both CtIP-AHA expressing clones (Fig. 5E and Supplemental Fig. 8E), indicating that the DNA-binding ability of CtIP is a critical determinant of resection-dependent DSB repair by HR. Collectively, these findings establish that CtIP-DNA interaction via the 'RHR' motif promotes efficient recruitment of CtIP to DSBs, thereby facilitating DNA-end resection and HR in human cells.

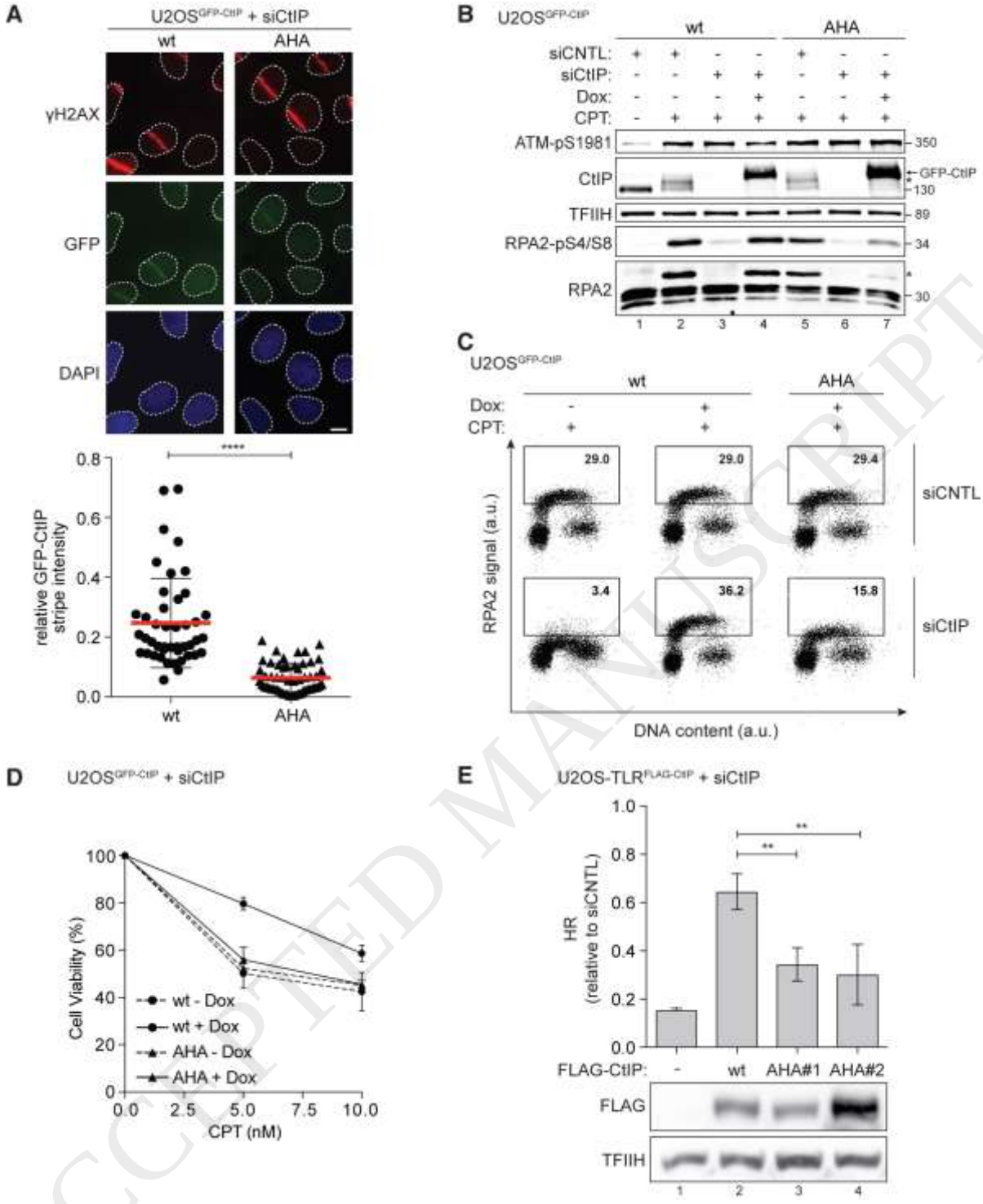

Fig. 5: Mutation of the RHR motif impairs CtIP accumulation at DSBs, DNA-end resection and HR. (A) U2OS clones harbouring inducible wt and AHA mutant GFP-CtIP were transfected with siCtIP for 48 h. 24 h later, cells were grown on coverslips in the presence of doxycycline (Dox) and BrdU for 24 h prior to laser micro-irradiation. 20 min post-irradiation, cells were fixed, immunostained for γH2AX and counterstained with DAPI for DNA and analysed by fluorescence microscopy. Upper panel, representative images. Scale bar, 10 µM. Lower panel, scatter plot of relative fluorescent intensities of GFP-CtIP laser stripes normalized to γH2AX stripe intensity (see Supplemental Fig. 6C). Data are presented as the mean (indicated by red bars) ± SD. Statistical difference was determined by Mann-Whitney test; **** ($P < 0.0001$). For each condition, more than 20 cells from two independent experiments were quantified. **(B)** The same cells as described in **(A)** transfected with control (CNTL) or CtIP siRNA were cultivated for 24 hr in absence (-) or presence (+) of Dox. 48 h post siRNA-transfection, cells were mock-treated (lane 1) or treated with CPT (1 µM) for 1 h and whole cell lysates were analysed by immunoblotting using the indicated antibodies. Asterisks indicate hyperphosphorylated forms

of endogenous CtIP and RPA2, respectively. **(C)** The same cells as described in **(B)** were treated with with CPT (1 µM) for 1 h and harvested for FACS analysis. Dot plots show fluorescent intensities (a.u., arbitrary units) of RPA2 signals (y-axis) against the DNA content (x-axis). Quantification gates were established in untreated samples and the percentages of cells within the gates are indicated. One representative out of three experiments with similar results is shown. **(D)** The same cells as described in **(A)** were treated with indicated doses of CPT and survival was determined after 4 days using the CellTiter-Blue® cell viability assay. Data are represented as the mean ± SD (n = 3). **(E)** HR events were quantified in stable U2OS-TLR clones expressing siRNA resistant FLAG-CtIP-wt or -AHA (two different clones). Cells were transfected with siCtIP and 8 h later co-transfected with IFP-I-SceI nuclease and BFP-Donor expression plasmids. 72 h post-siRNA transfection, cells were harvested for flow cytometry and immunoblot analysis. Data are represented as the mean ± SD (n = 3). Statistical differences were determined by ordinary one-way ANOVA test; ** ($P < 0.005$).

3. Discussion

3.1. PtCtIP represents a miniature ortholog of the CtIP protein family

Spontaneous or damage-induced DSBs need to be accurately repaired to maintain genome integrity and suppress tumorigenesis. During meiosis, however, hundreds of DBSs are deliberately induced by Spo11-dependent cleavage and subsequently repaired by homologous recombination to generate genetic diversity. In mammalian cells, faithful processing of both accidental and programmed DSBs requires the concerted action of the MRN complex and CtIP. Remarkably, while Mre11 and Rad50 are highly conserved and present throughout evolution, CtIP-related proteins have so far only been identified in eukaryotes [52,53]. Moreover, CtIP homologs have rapidly diverged in primary sequence and size ranging from 294 aa (*S. pombe* Ctp1) to 897 aa (human CtIP). In this study, we have characterized the genetic and biochemical activities of *P. tetraurelia* CtIP (PtCtIP), with only 198 aa in size, representing the smallest member of the Sae2/Ctp1/CtIP protein family known to date. Our primary sequence analysis revealed that PtCtIP is basically composed of the two hallmark structural elements common to all CtIP proteins: an N-terminal coiled-coil domain critical for dimer/tetramer assembly and a highly conserved C-terminus harboring a short linear motif implicated in DNA binding (Fig. 1 and Supplemental Fig. 1). In contrast, the large, intrinsically disordered middle region in human CtIP, shown to coordinate multiple protein-protein interactions and to harbor nuclease motifs [8,54], is strongly contracted in PtCtIP, comprising less than 50 amino acids (Fig. 1 and Supplemental Fig. 1). Nonetheless, the miniature PtCtIP is fully functional for HR-mediated repair of meiotic DSBs, emphasizing the interest of this homolog as a model to disentangle the core function of the CtIP-MR machinery from other regulatory functions.

3.2. P. tetraurelia contains two paralogous CtIP genes required for completion of meiotic recombination

An essential role for CtIP-related proteins in DSB repair was first described in *S. cerevisiae*, where Sae2 acts in concert with MRX to remove Spo11-oligonucleotide complexes from DSB ends during meiosis [12,13]. Consequently, Mre11 nuclease-deficient and *sae2*Δ mutant yeast strains fail to sporulate. Similar meiotic recombination defects were later observed for CtIP mutants in *S. pombe*, *A. thaliana*, *C. elegans*, and *T. thermophila* [9-11,43]. Furthermore, spore viability of 'CtIP' mutant cells could be partially rescued in a Spo11-deficient background in most species, indicating that it functions downstream of Spo11 in the repair of meiotic DSBs [29].

Due to a recent whole genome duplication event [37], two closely related CtIP gene copies, *PtCtIPa* and *PtCtIPb*, were identified in the model ciliate *P. tetraurelia* [38]. Interestingly, we found that *PtCtIPa* and *PtCtIPb* gene expression profiles are comparable to that of *PtSPO11* and *PtMRE11b*, displaying highest mRNA transcript levels in early meiosis (Fig. 2A and B). Simultaneous silencing of both PtCtIP genes impaired the recovery of functional new MACs in sexual progeny to a similar extent as Mre11b or Spo11 knockdowns (Fig. 2C), indicative of an essential function of PtCtIP during meiotic recombination. Specifically, we show that PtCtIP knockdown cells exhibit a defect in the progression of meiosis I with complete absence of new developing MACs at late stages of the sexual cycle (Fig. 3). Strikingly, *PtCtIP* disruption in a Spo11-deleted strain partially restored the physical development of new, yet non-viable MACs (Fig. 3B and Supplemental Fig. 4A), establishing that PtCtIP is a *bona fide* ortholog of Sae2/Ctp1/CtIP.

3.3. The RHR motif is critical for PtCtIP DNA-binding and DSB resection in human cells

We demonstrated that purified recombinant PtCtIP preferentially recognizes branched (or flap) DNA substrates through a highly conserved RHR motif located at the C-terminus in all CtIP homologs (Fig. 4) [7]. Our gel shift assays further suggested that PtCtIP binds to DNA in a multimeric state, giving rise to a high molecular weight complex. These results are in line with structural studies establishing an N-terminal tetrameric oligomerization scaffold in Ctp1 and CtIP [6,7], core residues of which are conserved in the PtCtIP protein sequence. Remarkably, while being unable to cleave DNA on its own, PtCtIP interacts with recombinant human MR complex, indicative of an evolutionary conserved protein-protein interaction module.

It has been reported that mutations of the RHR motif in Ctp1 resulted in an intermediate level of DNA damage sensitivity in *S. pombe* strains, suggesting that additional factors can partially compensate for DNA-binding defects [7]. Here, we provided evidence that mutation

of the RHR motif in human CtIP abrogates its spatial redistribution in response to DNA damage, supporting the importance of the DNA-binding activity across different species (Fig. 5A). In addition, we observed that human cells expressing a CtIP-AHA DNA-binding mutant display DNA-end resection and HR defects, ultimately resulting in profound hypersensitivity to CPT treatment (Fig. 5B-E). Notably, however, PtCtIP-AHA mutant is proficient for interacting with MR as well as for stimulating MR-dependent DNA cleavage *in vitro* (Supplemental Fig. 6C-E), suggesting that the DNA-binding function of CtIP proteins is mechanistically separable from MR activation in DSB repair processes. Similarly, it was reported that DNA-binding of Sae2 is not necessary for the stimulation of the MRX endonuclease [15].

In conclusion, our study provides converging evidence that the minimal *Paramecium* CtIP ortholog, being deprived of most of the regulatory motifs found in other CtIP protein species, has retained the ability to repair Spo11-induced meiotic DSBs. Our combined biochemical and functional analyses further imply that the DNA-binding activity of CtIP-related proteins is critical for the maintenance of genomic stability, perhaps by promoting the accumulation and correct assembly of CtIP tetramers at DSBs. Clearly, further investigations are required to elucidate how CtIP structurally integrates with the MR complex to promote efficient repair of DSBs. We propose that the trimmed-down PtCtIP might provide an ideal source for high-resolution structural analyses aiming to answer this question.

4. Materials and methods

4.1. Bioinformatics analysis of protein sequences

Due to the high sequence divergence among eukaryotic CtIP orthologs, a hierarchical approach was used to build the global alignment. First, six sequence profiles were independently generated from the full sequences of CtIP proteins in vertebrates (35 sequences), nematodes (10 sequences), plants (16 sequences), arthropods (19 sequences), protozoa (15 sequences) and fungi (63 sequences) using the MAFFT v7.0 algorithm with the E-INS-i iterative refinement method [55]. Next, using the HHsearch algorithm [56], these profiles were hierarchically aligned together resulting in a large multiple sequence alignment of 158 protein sequences. From this alignment, 35 sequences from model organisms were extracted and trimmed so that only the most conserved C-terminal domain was considered for the phylogenetic tree reconstruction. Phylogenetic tree was calculated using the PhyML algorithm [57] focusing on the C-terminal domain spanning residues 122-198 of PtCtIP with standard parameters (LG model of amino acids substitution, discrete gamma model with 6 categories and gamma shape factor of 1.729). Representation of the tree was performed using Dendroscope 3 [58]. Coiled-coil predictions were performed using PCOILS [59].

4.2. P. tetraurelia strains, cultivation, and gene silencing

Autogamy and conjugation experiments were carried out at 27°C with strain 51new [60]. Cells were grown in a wheat grass powder (WGP, Pines International Inc.) infusion medium bacterized the day before use with *Klebsiella pneumoniae* and supplemented with 0.8 µg/ml β-sitosterol. The somatic *SPO11* knockout was generated as described previously [61]. In brief, following conjugation of reactive 51new cells from mating types 7 (mt7) and 8 (mt8), stable mating pairs were transferred to WGP medium inoculated with *Escherichia coli* HT115 bacteria harbouring plasmid PtSPO11-1 and induced for dsRNA production [33].

For RNAi-mediated gene silencing experiments during autogamy, cells were grown for 20 to 25 vegetative divisions under standard conditions, before transfer to WGP medium inoculated with HT115 bacteria harbouring the appropriate dsRNA-producing plasmids [62]. To monitor the progression of autogamy, cells were permeabilized and fixed prior to DAPI staining as described [35]. Nuclear developmental stages were observed using a Zeiss Axioplan 2 Imaging epifluorescence microscope with 63x/1.4 Plan-Apochromate or 40x/1.3 Plan-Neofluar oil objectives. The capability of sexual progeny to develop a functional new MAC was monitored following individual transfer of 30 autogamous cells to standard culture medium [32].

RNAi experiments during conjugation were performed as described [33]. In brief, reactive 51new mt7 and mt8 cells were prepared in each RNAi medium and mixed to start conjugation. Following 1.75 h incubation at 27°C, freshly induced RNAi medium was added to the mix to synchronize conjugation. Mating pairs were transferred manually to each RNAi medium and incubated at 27°C to complete MAC development and resume vegetative growth. To monitor sexual processes, conjugating cells were permeabilized, fixed and processed for immunostaining as described [34]. To reveal micronuclei and the zygotic nucleus during conjugation, cells were incubated for 1 h with primary anti-γ-tubulin antibodies (1:400, [45]), then washed with TBST (10 mM Tris-HCl pH 7.4, 0.15 M NaCl, 0.1% Tween) + 3% BSA prior to 15 min incubation with secondary Alexa Fluor 488-conjugated anti-rabbit antibodies (1:300, ThermoFisher Scientific), followed by DAPI staining. Imaging was performed using a Zeiss Axioplan 2 Imaging epifluorescence microscope with a 63x/1.4 Plan-Apochromate oil objective.

4.3. dsRNA-producing plasmids for silencing P. tetraurelia genes

All RNAi plasmids are derivatives of vector L4440 [63] and carry a target gene fragment between two convergent T7 promoters. Each insert was chosen in order to minimize the risk of cross-silencing by using the "RNAi off-target" tool of ParameciumDB [38]. Plasmids p0ND7c [64], pICL7a [65] and pL4440-SPO11-1 [33] were used to target *Paramecium ND7, ICL7a* and *SPO11* genes, respectively. RNAi plasmids targeting *PtCtIP* and *PtMRE11* genes were constructed as follows: pL4440-PtCtIPa: a 354-bp fragment from *PtCtIPa* (nt 266-619) was amplified by PCR from total genomic DNA from *P. tetraurelia*, using primers PtCtIPa-SpeI-F and PtCtIPa-SpeI-R (Supplemental Table S1) and the Phusion High-Fidelity DNA polymerase (New England Biolabs). Following SpeI-restriction, the PCR fragment was inserted into the unique XbaI site of vector L4440. pL4440-PtCtIPb: same cloning procedure for a 354-bp fragment from *PtCtIPb* (nt 266-619) amplified using primers PtCtIPb-SpeI-F and PtCtIPb-SpeI-R. pL4440-PtMRE11a1: same cloning procedure for a 492-bp fragment from *PtMRE11a* (IF2: nt 1422-1913) amplified using primers PtMRE11a1-SpeI-F and PtMRE11a1-SpeI-R. pL4440-PtMRE11b1: same cloning procedure for a 510-bp fragment from *PtMRE11b* (IF2: nt 1420-1929) amplified using primers PtMRE11b1-SpeI-F and PtMRE11b1-SpeI-R. pL4440-PtMRE11a2: same cloning procedure for a 507-bp fragment from *PtMRE11a* (IF1: nt 24-530) amplified using primers PtMRE11a2-SpeI-F and PtMRE11a2-SpeI-R. The IF1 sequence from *PtMRE11a* cross-reacts with *PtMRE11b*. pL4440-PtMRE11b2: same cloning procedure for a 508-bp fragment from *PtMRE11b* (IF1:

nt 24-531) amplified using primers PtMRE11b2-SpeI-F and PtMRE11b2-SpeI-R. The IF1 sequence from *PtMRE11b* cross-reacts with *PtMRE11a*.

4.4. Northern blot analysis

Total RNA was extracted from ~400,000 cells for each indicated time point during autogamy of 51new cells grown in standard *K. pneumoniae* medium and processed for northern blot hybridization using ^{32}P-labeled probes as described [33]. Unless otherwise stated, PCR fragments of *PtSPO11*, *PtCtIPa*, *PtCtIPb*, *PtMRE11a* and *PtMRE11b* RNAi-targeting plasmids were used as gene-specific double-stranded probes (Supplemental Table S1). The sequence of the 17S rRNA oligonucleotide probe is shown in Supplemental Table S1. Hybridization signals were collected using a Typhoon TRIO Variable Mode Phosphorimager (GE Healthcare). Quantification was performed using the ImageJ software and mRNA levels were normalized relative to 17S rRNA hybridization signals.

4.5. Cloning, expression and purification of recombinant PtCtIPa

The *PtCtIPa* open reading frame (NCBI database GI accession number 145537105) was synthesized, cloned into pUC57 and verified by sequencing (GeneScript, Piscataway, NJ, USA). *PtCtIPa* was PCR-amplified using the primers listed in Supplemental Table S1 and cloned into the pFastBac(FB)-MBP-His vector. PtCtIPa-R181A/R183A amino acids substitutions were generated by site-directed mutagenesis using PfuTurbo DNA polymerase (Agilent Technologies) and appropriate primers (Supplemental Table S1). Recombinant PtCtIPa proteins were expressed using the pFB-MBP-PtCtIP-His vectors and the Bac-to-Bac baculovirus expression system (Invitrogen) in insect cells as described previously [66]. In brief, Sf9 cells ($1x10^6$ cells/ml) cultured in HyClone SFX-Insect cell culture medium (GE Healthcare) were transduced with high-titer viruses and grown for 52 h at 27°C. All subsequent steps were performed at 4°C. Pellets of 200 ml cultures were resuspended in lysis buffer (50 mM Tris-HCl, pH 7.5, 1 mM EDTA, 1 mM DTT, 1 x Halt Protease Inhibitor Cocktail (Thermo Scientific), 1 mM PMSF, 30 µg/ml leupeptin) and incubated stirring for 20 min before adding 0.5 volumes of 50% glycerol. 5 M NaCl was added dropwise to the sample, to reach a final concentration of 300 mM NaCl, and the solution was incubated 30 min before centrifugation at 38,000 g for 30 min. Soluble extracts were bound to pre-equilibrated amylose resin (New England Biolabs, UK) for 1 h and the resin was washed with wash buffer (50 mM Tris-HCl, pH 7.5, 1 M NaCl, 10% Glycerol, 1 mM PMSF, 2 mM β-mercaptoethanol, 10 µg/ml leupeptin). Proteins were eluted with wash buffer containing 10 mM maltose. To

cleave the MBP tag, samples were incubated for 3 h with recombinant prescission protease (PP) expressed in *E. coli* and purified using standard procedures [18]. Next, imidazole was added to a final concentration of 20 mM before adding 0.5 ml Ni-NTA-agarose (Qiagen). The resin was extensively washed with NTA buffer (50 mM Tris-HCl, pH 7.5, 150 mM NaCl, 10% glycerol, 0.5 mM PMSF, 2 mM β-mercaptoethanol, 10 mM imidazole) and proteins eluted with NTA buffer supplemented with 400 mM imidazole. Peak fractions containing PtCtIPa-His were incubated with amylose resin to remove the remaining uncleaved MBP-tagged PtCtIPa, pooled, and dialysed against dialysis buffer (50 mM Tris-HCl, pH 7.5, 300 mM NaCl, 10% glycerol, 0.5 mM PMSF and 5 mM β-mercaptoethanol). Small aliquots of the purified PtCtIPa proteins were snap frozen and stored at -80°C. Recombinant human CtIP and Mre11-Rad50 (MR) complex were expressed and purified as described previously [67].

4.6. Cloning, expression and purification of recombinant human CtIP-CTD

The CtIP C-terminal domain (CTD) spanning amino acid residues 608-897 was PCR-amplified from Flag-CtIP-wt and R837A/R839A plasmids (described in 4.12) using primers listed in Supplemental Table S1 and cloned into pET28-MBP-TEV vector (Addgene: #69929) downstream of the TEV cleavage site. Constructs were expressed in BL21-CodonPlus-RIL *E. coli* by growing them for 20 h at 18°C using 0.5 mM IPTG. Bacterial pellets were resuspended in lysis buffer (50 mM Tris pH 8.0, 300 mM NaCl, 0.5 mM zinc acetate) and snap frozen. After thawing, 1 mM PMSF, protease inhibitor cocktail (cOmplete, EDTA-free, Sigma), 2 mM β-mercaptoethanol and 0.1 mg/ml lysozyme was added and lysates were stirred at 4°C for 15 min. Subsequently, lysates were sonicated for 5 min and insoluble material was removed by ultracentrifugation at 125,000 g for 1 h. Fusion proteins were purified from clarified lysates through amylose affinity chromatography (5 ml MBPTrap HP, GE Healthcare) and elution with 20 mM Tris pH 8.0, 2 mM β-mercaptoethanol, 300 mM NaCl, 2 M methyl α-D-glucopyranoside (Sigma). Prior to cleavage with TEV protease, buffer exchange into 20 mM Tris pH 8.0, 300 mM NaCl, 5 mM β-mercaptoethanol was performed using a HiPrep 26/10 Desalting column (GE Healthcare). Proteins were concentrated to 2 mg/ml using Amicon Ultra 10’000 MWCO centrifugal filter units (Millipore) and MBP-tagged TEV protease (Gene and Cell Technologies) was added in a ratio of 1:5. Cleavage was performed overnight at 20°C and unwanted protein species were captured by amylose affinity chromatography. Further purification of amylose chromatography flow-through was achieved through size-exclusion chromatography (HiLoad

16/600 Superdex 75, GE Healthcare) in 20 mM Tris pH 8.0, 150 mM NaCl, 5 mM β-mercaptoethanol.

4.7. Size exclusion chromatography (SEC)

Approximately 25 µg of purified PtCtIPa proteins, 50 µg of purified Ctp1 or 50 µg of purified MBP (Prospec) were loaded at 0.5 ml/min onto a Superose 6 10/300 GL size exclusion chromatography column (GE Healthcare) in 50 mM Tris-HCl, pH 7.5, 300 mM NaCl, 10% glycerol, 0.5 mM PMSF and 5 mM β-mercaptoethanol using an ÄKTA™ Pure chromatography system (GE Healthcare).

4.8. DNA substrates

The sequences of 50mer oligonucleotides used in DNA binding and nuclease assays are listed in Supplemental Table S1. Where indicated, the 5' end was labeled with T4 polynucleotide kinase (PNK; New England Biolabs) in the presence of [γ-^{32}P]-ATP, while 3' end-labeling was performed with terminal deoxynucleotidyl transferase (TdT; New England Biolabs) in the presence of [α-^{32}P]-cordycepin-5'-triphosphate. Unincorporated nucleotides were removed using MicroSpin G25 columns (GE Healthcare). The double-stranded oligo substrates were annealed by heating the oligonucleotides at 95°C and slow gradual cooling to room temperature in either 1x TdT or PNK buffer.

4.9. DNA binding and competition assays

All steps were performed at 4°C under native conditions. Recombinant proteins were incubated with 10 nM of the indicated radiolabeled DNA substrates for 20 min at 20°C in 20 µl binding buffer (20 mM Tris-HCl, pH 7.5, 10 mM NaCl, 0.5 mM DTT, 10 µg/ml BSA, 4% glycerol). Protein-DNA complexes were separated on a 4-20% TBE precast gel (Novex) for 120 min at 100 V, respectively, dried and exposed to a phosphor screen before imaging using a Typhon FLA 9500 scanner (GE Healthcare). Data were quantified with ImageQuant TL software (GE Healthcare). In competition experiments, PtCtIPa proteins were incubated with radiolabeled DNA substrates for 5 min on ice prior to the addition of increasing amounts of cold, blunt-ended competitor 61mer dsDNA (Supplemental Table S1). DNA binding assays with recombinant human CtIP-CTD proteins were performed as previously described [6]. In brief, CtIP-CTD-wt and -AHA mutant were incubated with 1 µM fluorescein-labeled 50mer dsDNA for 1 h at 21°C and loaded onto 1.2 % agarose gel (in 0.5x TBE buffer). Gel was run

in 0.5 x TBE buffer at 25 V for 3 h at 4°C. DNA was visualized using Typhoon FLA 9500 FluorImager. Data were quantified with ImageJ software.

4.10. DNA cleavage assays

Recombinant proteins were incubated with 10 nM of 5' or 3' radiolabeled DNA substrates for 60 min at 37°C in 10 µl reaction buffer (20 mM Tris-HCl, pH 7.5, 10 mM NaCl, 0.5 mM DTT, 10 µg/ml BSA, 4% glycerol) supplemented with either 5 mM $MgCl_2$ or 1 mM $MnCl_2$. 10 nM of purified recombinant human DNA2 was used as a control. Nuclease reactions were stopped by adding an equal volume of 80% formamide loading dye. Samples were boiled for 5 min and products were separated on a 20% polyacrylamide gel containing 7 M urea. Gels were fixed in 1x TBE buffer containing 10% acetic acid, 50% EtOH and 10% glycerol for 20 min, dried and exposed to a phosphor screen before imaging on a Typhoon FLA 9500 scanner (GE Healthcare). Nuclease assays using PhiX174 single-stranded circular (ssc) DNA as a substrate was performed as described previously [14]. In brief, 85 ng of PhiX174 virion DNA was incubated with recombinant proteins for 2 h at 37°C in 10 µl reaction buffer (30 mM potassium/MOPS, pH 7.2, 1 mM DTT, 1 mM ATP, 25 mM KCl, 25 ng/ul BSA) supplemented with 5 mM of either $MgCl_2$ or $MnCl_2$. Reactions were stopped by adding 0.5 µl Proteinase K (20.6 mg/ml, Roche) and 4 µl stop solution (2% SDS, 50 mM EDTA) for 20 min at room temperature. Samples were run on a 0.8% TAE agarose gel for 1 h at 80 V, stained with SYBR Gold Nucleic Acid Gel Stain (Molecular Probes) for 20 min and the gel was imaged using a Typhoon FLA 9500 scanner. Data were quantified with ImageQuant TL software.

4.11. MBP pull-down assay

Soluble protein extracts of Sf9 cells expressing MBP alone or MBP-PtCtIPa-His were incubated with amylose resin for 1 h at 4°C. Resin was washed three times with NTEN buffer (20 mM Tris-HCl, pH 7.4, 0.1 mM EDTA, 0.5% NP-40) containing 300 mM NaCl and once with TEN100 buffer (20 mM Tris-HCl, pH 7.4, 0.1 mM EDTA, 100 mM NaCl). MBP proteins coupled to amylose beads were mixed with 0.5 µg of recombinant human Mre11-Rad50 (MR) complex for 2 h at 4°C. Beads were washed with NTEN buffer containing 500 mM NaCl and proteins were eluted in TEN100 buffer containing 20 mM maltose. Samples were analysed by SDS-PAGE followed by immunoblotting.

4.12. Plasmids, antibodies and siRNA

The pcDNA5/FRT/TO-GFP-CtIP-wild type (wt) and 3x Flag-CtIP-wt expression vectors were described previously [6,51]. CtIP-R837A/R839A amino acids substitutions were generated by site-directed mutagenesis using PfuTurbo DNA polymerase and appropriate primers (Supplemental Table S1). All CtIP constructs are siRNA-resistant [14]. Antibodies for immunoblotting were: anti-FLAG M2 (Sigma F3165, 1:1000), anti-GFP (Santa Cruz B-2, 1:1000), anti-Mre11 (GeneTex 12D7, 1:1000), anti-Rad50 (GeneTex 13B3, 1:1000), anti-TFIIH p89 (Santa Cruz S-19, 1:1000), anti-RPA2 (Calbiochem NA19L, 1:1000), anti-phospho RPA2 (S4/S8) (Bethyl A300-245A, 1:5000), anti-phospho ATM (S1981) (Abcam ab81292, 1:5000). Control siRNA (luciferase 5′-CGUACGCGGAAUACUUCGA-3′) and CtIP siRNA (5′-GCUAAAACAGGAACGAAUC-3′) [14] were purchased from Microsynth.

4.13. Cell lines, cell culture, transfections and treatments

U2OS cells were maintained in Dulbecco's modified Eagle's medium (DMEM) supplemented with 10% fetal calf serum (FCS), 100 U/ml penicillin and 100 mg/ml streptomycin. The Flp-In T-REx system (Invitrogen Life Technologies) was used to generate U2OS cells stably expressing siRNA-resistant GFP-tagged CtIP-wt or CtIP-R837A/R839A under the control of a doxycycline-inducible promoter. In brief, pcDNA5/FRT/TO-GFP-CtIP and the Flp recombinase expression plasmid, pOG44, were mixed in a 1:9 ratio and transfected into U2OS Flp-In T-REx cells. 24 h later, cells were plated at different dilutions and 48 h post-transfection the medium was supplemented with 250 mg/ml hygromycin B and 12.5 mg/ml blasticidin S. The medium was replaced every 2–3 days and cells were selected for approximately 14 days. Resistant colonies were picked and single-cell clones analysed for GFP expression by immunoblotting and immunofluorescence microscopy after 24 h induction of protein expression with 1 µg/ml doxycycline (Dox, Sigma-Aldrich). The CtIP-R837A/R839A mutation in stable U2OS cells was verified by genomic sequencing. U2OS-TLR cells [6] stably transfected with Flag-tagged versions of CtIP were grown in the presence of 0.5 µg/ml puromycin and 0.5 mg/ml geneticin. Plasmid transfections were performed using the Fugene 6 transfection reagent (Promega) according to the manufacturer's instructions. siRNA transfections were performed using Lipofectamine RNAiMax (Life Technologies) according to the manufacturer’s instructions. Camptothecin (CPT) was purchased from Sigma. Laser micro-irradiation was performed as described previously [51]. In brief, cells were grown in medium supplemented with 10 µM BrdU for 24 h. Cells were microirradiated using a MMI CELLCUT system containing a UVA laser of 355 nM

(Molecular Machines and Industries). The laser intensity was set to 50% energy output and each cell was exposed to the laser beam for 300 ms.

4.14. Immunofluorescence microscopy

Cells grown on coverslips were fixed directly in formaldehyde (4%, w/v in PBS) for 15 min and permeabilized for 5 min in 0.5% Triton X-100 in PBS. Cells were incubated for 1 h with primary anti-H2AX-pS139 antibody (Cell Signalling 20E3, 1:500), followed by 1 h incubation with secondary Alexa Fluor 594-conjugated anti-rabbit antibody (Life Technologies, 1:1000). Coverslips were mounted with Vectrashield® (Vector Laboratories) containing DAPI and imaged using a Leica DM6B fluorescence microscope at 63X magnification.

4.15. DNA-end resection assay

Flow cytometry-based resection assay was performed as described previously [51]. Briefly, U2OS cells were transfected with CtIP siRNA. Where indicated, 24 h post-transfection, doxycycline was added to the cells to induce the expression of GFP-CtIP. 48 h post-transfection, cells were either mock-treated or treated for 1 h with 1 μM CPT. Cells were harvested, pre-extracted with 0.3% Triton-X100 in PBS for 15 min on ice and fixed with 4% formaldehyde (w/v) for 10 min at room temperature. Cells were incubated for 1 h with anti-RPA2 antibody (Calbiochem NA19L, 1:100) or anti-H2AX-pS139 antibody (Cell Signalling 20E3, 1:200), followed by 30 min incubation with Alexa Fluor 647- or 488-conjugated secondary antibody (Life Technologies, 1:250) and counterstained with DAPI/RNase. Samples were analysed by flow cytometry on a CyAn ADP 9 (Dako). Data analysis was performed using FlowJo X software (Tree Star).

4.16. CellTiter-Blue® Cell viability assay

Cell viability was measured as previously described [51]. Briefly, U2OS clones stably expressing doxycycline-inducible siRNA-resistant forms of GFP-CtIP were transfected with indicated siRNAs. 24 h post-transfection, cells were seeded in triplicates at a density of 500 cells/well in a 96-well plate in medium supplemented with 1 μg/ml doxycycline. 24 h later, cells were continuously treated with indicated doses of CPT and grown for 4 days at 37°C. To measure viability, CellTiter-Blue® reagent (Promega) was added on the last day and incubated for 4 h at 37°C before fluorescence was measured at 560/590 nm using a microplate reader (Molecular Devices).

4.17. Homologous recombination reporter assay

Homologous recombination (HR) was measured using the TLR assay as described [6]. In brief, U2OS-TLR cells stably expressing siRNA-resistant forms of 3xFLAG-CtIP were seeded at a density of 500'000 cells per 6-cm dish. 6 h after siRNA transfection, cells were co-transfected with 2 μg of BFP donor and 3 μg of IFP-*I-SceI* endonuclease plasmids. 3 days after siRNA transfection, cells were harvested, fixed in 2% paraformaldehyde/PBS for 20 min at room temperature, washed and resuspended in 300 ul of PBS supplemented with 1 mg/ml BSA. Flow cytometry analysis was performed using the LSR-Fortessa Cell Analyzer (BD Biosciences). A minimum of 10,000 BFP/IFP double-positive cells were scored for GFP signal representing HR. Data analysis was performed using FlowJo X software (Tree Star).

Conflict of interest statement

The authors declare that there is no conflict of interest.

Funding

This work was supported by the Swiss National Science Foundation [grant numbers 31003A_135507, 31003A_156023, and 31003A_176161, all to A.A.S.]; the Swiss Cancer League [grant number KFS-3845-02-2016-R to A.A.S.]; the Centre National de la Recherche Scientifique (CNRS) [intramural funding to M.B.], the ARC Foundation for Cancer Research [grant number SFI20121205487 to M.B.] and the French National Agency for Research (ANR) [grant number ANR-14-CE10-0005-01 to M.B., grant number ANR-15-CE110008-01 to R.G.]. The funders had no role in study design, data collection and analysis, decision to publish, or preparation of the manuscript.

Acknowledgements

We would like to thank Cindy Mathon and Pascaline Tirand for excellent technical assistance and Loïc Escoriza, Nathalie Mathy and Coralie Zangarelli for their help in the handling of *Paramecium* cultures. Anti-γ-tubulin antibodies were kindly provided by Janine Beisson and Anne-Marie Tassin (I2BC, Gif-sur-Yvette, France). We thank Pavel Janscak (University of Zurich, Switzerland) for providing purified recombinant human CtIP and Mre11-Rad50 complex and for experimental advice. We thank Petr Cejka (Institute for Research in Biomedicine, Bellinzona, Switzerland) for providing pFastBac-MBP-His vector,

pGEX-1T-GST-PP expression construct and purified recombinant human DNA2. Purified recombinant *S. pombe* Ctp1 protein was a kind gift of Scott Williams (National Institute of Environmental Health Sciences, US National Institutes of Health, Research Triangle Park USA). Anti-phospho CtIP (T847A) antibodies were kindly provided by Markus Löbrich (Darmstadt University of Technology, Darmstadt, Germany). We acknowledge Stephen P. Jackson (Wellcome Trust Cancer Research UK Gurdon Institute, University of Cambridge, UK) for providing U2OS-TLR cells and FLAG-CtIP expression plasmid and Daniel Durocher (University of Toronto, Canada) for sharing U2OS Flp-In T-REx cells.

Appendix A. Supplementary data

References

1. Hanahan D, Weinberg RA. Hallmarks of cancer: the next generation. Cell. 2011;144: 646–674. doi:10.1016/j.cell.2011.02.013

2. Pommier Y, Sun Y, Huang S-YN, Nitiss JL. Roles of eukaryotic topoisomerases in transcription, replication and genomic stability. Nat Rev Mol Cell Biol. 2016;17: 703–721. doi:10.1038/nrm.2016.111

3. Chang HHY, Pannunzio NR, Adachi N, Lieber MR. Non-homologous DNA end joining and alternative pathways to double-strand break repair. Nat Rev Mol Cell Biol. 2017;18: 495–506. doi:10.1038/nrm.2017.48

4. Jasin M, Rothstein R. Repair of strand breaks by homologous recombination. Cold Spring Harb Perspect Biol. 2013;5: a012740. doi:10.1101/cshperspect.a012740

5. Symington LS. Mechanism and regulation of DNA end resection in eukaryotes. Crit Rev Biochem Mol Biol. 2016;51: 195–212. doi:10.3109/10409238.2016.1172552

6. Davies OR, Forment JV, Sun M, Belotserkovskaya R, Coates J, Galanty Y, et al. CtIP tetramer assembly is required for DNA-end resection and repair. Nat Struct Mol Biol. 2015;22: 150–157. doi:10.1038/nsmb.2937

7. Andres SN, Appel CD, Westmoreland JW, Williams JS, Nguyen Y, Robertson PD, et al. Tetrameric Ctp1 coordinates DNA binding and DNA bridging in DNA double-strand-break repair. Nat Struct Mol Biol. 2015;22: 158–166. doi:10.1038/nsmb.2945

8. Andres SN, Williams RS. CtIP/Ctp1/Sae2, molecular form fit for function. DNA Repair (Amst). 2017;56: 109–117. doi:10.1016/j.dnarep.2017.06.013

9. Penkner A, Portik-Dobos Z, Tang L, Schnabel R, Novatchkova M, Jantsch V, et al. A conserved function for a Caenorhabditis elegans Com1/Sae2/CtIP protein homolog in meiotic recombination. The EMBO Journal. 2007 ed. 2007;26: 5071–5082. doi:10.1038/sj.emboj.7601916

10. Uanschou C, Siwiec T, Pedrosa-Harand A, Kerzendorfer C, Sanchez-Moran E, Novatchkova M, et al. A novel plant gene essential for meiosis is related to the human CtIP and the yeast COM1/SAE2 gene. The EMBO Journal. 2007 ed. 2007;26: 5061–5070. doi:10.1038/sj.emboj.7601913

11. Limbo O, Chahwan C, Yamada Y, de Bruin RA, Wittenberg C, Russell P. Ctp1 is a cell-cycle-regulated protein that functions with Mre11 complex to control double-strand break repair by homologous recombination. Mol Cell. 2007 ed. 2007;28: 134–146. doi:10.1016/j.molcel.2007.09.009

12. McKee AH, Kleckner N. A general method for identifying recessive diploid-specific mutations in Saccharomyces cerevisiae, its application to the isolation of mutants blocked at intermediate stages of meiotic prophase and characterization of a new gene SAE2. Genetics. 1997;146: 797–816.

13. Prinz S, Amon A, Klein F. Isolation of COM1, a new gene required to complete

meiotic double-strand break-induced recombination in Saccharomyces cerevisiae. Genetics. 1997;146: 781–795.

14. Sartori AA, Lukas C, Coates J, Mistrik M, Fu S, Bartek J, et al. Human CtIP promotes DNA end resection. Nature. 2007;450: 509–514. doi:10.1038/nature06337

15. Cannavo E, Cejka P. Sae2 promotes dsDNA endonuclease activity within Mre11-Rad50-Xrs2 to resect DNA breaks. Nature. 2014. doi:10.1038/nature13771

16. Paull TT, Gellert M. The 3“ to 5” exonuclease activity of Mre 11 facilitates repair of DNA double-strand breaks. Mol Cell. 1998;1: 969–979.

17. Paull TT, Gellert M. Nbs1 potentiates ATP-driven DNA unwinding and endonuclease cleavage by the Mre11/Rad50 complex. Genes Dev. 1999;13: 1276–1288.

18. Anand R, Ranjha L, Cannavo E, Cejka P. Phosphorylated CtIP Functions as a Co-factor of the MRE11-RAD50-NBS1 Endonuclease in DNA End Resection. Mol Cell. 2016;64: 940–950. doi:10.1016/j.molcel.2016.10.017

19. Garcia V, Phelps SEL, Gray S, Neale MJ. Bidirectional resection of DNA double-strand breaks by Mre11 and Exo1. Nature. 2011;479: 241–244. doi:10.1038/nature10515

20. Paudyal SC, Li S, Yan H, Hunter T, You Z. Dna2 initiates resection at clean DNA double-strand breaks. Nucleic Acids Res. Oxford University Press; 2017;45: 11766–11781. doi:10.1093/nar/gkx830

21. Mimitou EP, Symington LS. Sae2, Exo1 and Sgs1 collaborate in DNA double-strand break processing. Nature. 2008;455: 770–774. doi:10.1038/nature07312

22. Zhu Z, Chung W-H, Shim EY, Lee SE, Ira G. Sgs1 helicase and two nucleases Dna2 and Exo1 resect DNA double-strand break ends. Cell. 2008;134: 981–994. doi:10.1016/j.cell.2008.08.037

23. Nicolette ML, Lee K, Guo Z, Rani M, Chow JM, Lee SE, et al. Mre11-Rad50-Xrs2 and Sae2 promote 5' strand resection of DNA double-strand breaks. Nat Struct Mol Biol. 2010;17: 1478–1485. doi:10.1038/nsmb.1957

24. Niu H, Chung W-H, Zhu Z, Kwon Y, Zhao W, Chi P, et al. Mechanism of the ATP-dependent DNA end-resection machinery from Saccharomyces cerevisiae. Nature. 2010;467: 108–111. doi:10.1038/nature09318

25. Lam I, Keeney S. Mechanism and regulation of meiotic recombination initiation. Cold Spring Harb Perspect Biol. 2014;7: a016634. doi:10.1101/cshperspect.a016634

26. Arora S, Deshpande RA, Budd M, Campbell J, Revere A, Zhang X, et al. Genetic separation of Sae2 nuclease activity from Mre11 nuclease functions in budding yeast. Molecular and Cellular Biology. 2017;37: e00156-17. doi:10.1128/MCB.00156-17

27. Ma L, Milman N, Nambiar M, Smith GR. Two separable functions of Ctp1 in the early steps of meiotic DNA double-strand break repair. Nucleic Acids Res. 2015;43: 7349–7359. doi:10.1093/nar/gkv644

28. Lemmens BBLG, Johnson NM, Tijsterman M. COM-1 promotes homologous recombination during Caenorhabditis elegans meiosis by antagonizing Ku-mediated non-homologous end joining. PLoS Genetics. 2013;9: e1003276. doi:10.1371/journal.pgen.1003276

29. Hartsuiker E, Mizuno K, Molnar M, Kohli J, Ohta K, Carr AM. Ctp1CtIP and Rad32Mre11 nuclease activity are required for Rec12Spo11 removal, but Rec12Spo11 removal is dispensable for other MRN-dependent meiotic functions. Molecular and Cellular Biology. 2009;29: 1671–1681. doi:10.1128/MCB.01182-08

30. Hartsuiker E, Neale MJ, Carr AM. Distinct Requirements for the Rad32Mre11 Nuclease and Ctp1CtIP in the Removal of Covalently Bound Topoisomerase I and II from DNA. Mol Cell. Elsevier Inc; 2009;33: 117–123. doi:10.1016/j.molcel.2008.11.021

31. Arnaiz O, Mathy N, Baudry C, Malinsky S, Aury J-M, Denby Wilkes C, et al. The Paramecium germline genome provides a niche for intragenic parasitic DNA: evolutionary dynamics of internal eliminated sequences. PLoS Genetics. 2012;8: e1002984. doi:10.1371/journal.pgen.1002984

32. Kapusta A, Matsuda A, Marmignon A, Ku M, Silve A, Meyer E, et al. Highly Precise and Developmentally Programmed Genome Assembly in Paramecium Requires Ligase IV–Dependent End Joining. PLoS Genetics. 2011;7: e1002049. doi:10.1371/journal.pgen.1002049

33. Baudry C, Malinsky S, Restituito M, Kapusta A, Rosa S, Meyer E, et al. PiggyMac, a domesticated piggyBac transposase involved in programmed genome rearrangements in the ciliate Paramecium tetraurelia. Genes Dev. 2009;23: 2478–2483. doi:10.1101/gad.547309

34. Dubois E, Mathy N, Régnier V, Bischerour J, Baudry C, Trouslard R, et al. Multimerization properties of PiggyMac, a domesticated piggyBac transposase involved in programmed genome rearrangements. Nucleic Acids Res. 2017;45: 3204–3216. doi:10.1093/nar/gkw1359

35. Marmignon A, Bischerour J, Silve A, Fojcik C, Dubois E, Arnaiz O, et al. Ku-mediated coupling of DNA cleavage and repair during programmed genome rearrangements in the ciliate Paramecium tetraurelia. PLoS Genetics. 2014;10: e1004552. doi:10.1371/journal.pgen.1004552

36. Chi J, Mahé F, Loidl J, Logsdon J, Dunthorn M. Meiosis gene inventory of four ciliates reveals the prevalence of a synaptonemal complex-independent crossover pathway. Mol Biol Evol. 2014;31: 660–672. doi:10.1093/molbev/mst258

37. Aury J-M, Jaillon O, Duret L, Noel B, Jubin C, Porcel BM, et al. Global trends of whole-genome duplications revealed by the ciliate Paramecium tetraurelia. Nature. 2006;444: 171–178. doi:10.1038/nature05230

38. Arnaiz O, Sperling L. ParameciumDB in 2011: new tools and new data for functional and comparative genomics of the model ciliate Paramecium tetraurelia. Nucleic Acids Res. 2011;39: D632–6. doi:10.1093/nar/gkq918

39. Huertas P, Cortés-Ledesma F, Sartori AA, Aguilera A, Jackson SP. CDK targets Sae2 to control DNA-end resection and homologous recombination. Nature. 2008 ed. 2008;455: 689–692. doi:10.1038/nature07215

40. Huertas P, Jackson SP. Human CtIP mediates cell cycle control of DNA end resection and double strand break repair. J Biol Chem. 2009 ed. 2009;284: 9558–9565. doi:10.1074/jbc.M808906200

41. Wang H, Shi LZ, Wong CCL, Han X, Hwang PY-H, Truong LN, et al. The Interaction of CtIP and Nbs1 Connects CDK and ATM to Regulate HR-Mediated Double-Strand Break Repair. PLoS Genetics. 2013;9: e1003277. doi:10.1371/journal.pgen.1003277

42. Arnaiz O, Van Dijk E, Bétermier M, Lhuillier-Akakpo M, de Vanssay A, Duharcourt S, et al. Improved methods and resources for paramecium genomics: transcription units, gene annotation and gene expression. BMC Genomics. 2017;18: 483. doi:10.1186/s12864-017-3887-z

43. Lukaszewicz A, Howard-Till RA, Novatchkova M, Mochizuki K, Loidl J. MRE11 and COM1/SAE2 are required for double-strand break repair and efficient chromosome pairing during meiosis of the protist Tetrahymena. Chromosoma. 2010;119: 505–518. doi:10.1007/s00412-010-0274-9

44. Bétermier M, Duharcourt S, Seitz H, Meyer E. Timing of developmentally programmed excision and circularization of Paramecium internal eliminated sequences. Molecular and Cellular Biology. 2000;20: 1553–1561.

45. Klotz C, Ruiz F, Garreau de Loubresse N, Wright M, Dupuis-Williams P, Beisson J. Gamma-tubulin and MTOCs in Paramecium. Protist. 2003;154: 193–209.

46. Lisby M, Barlow JH, Burgess RC, Rothstein R. Choreography of the DNA damage response: spatiotemporal relationships among checkpoint and repair proteins. Cell. 2004;118: 699–713. doi:10.1016/j.cell.2004.08.015

47. Chen L, Nievera CJ, Lee AY-L, Wu X. Cell cycle-dependent complex formation of BRCA1.CtIP.MRN is important for DNA double-strand break repair. J Biol Chem. 2008 ed. 2008;283: 7713–7720. doi:10.1074/jbc.M710245200

48. Eid W, Steger Martin, El-Shemerly M, Ferretti LP, Peña-Diaz J, König C, et al. DNA end resection by CtIP and exonuclease 1 prevents genomic instability. EMBO Rep. 2010;11: 962–968. doi:10.1038/embor.2010.157

49. Kousholt AN, Fugger K, Hoffmann S, Larsen BD, Menzel T, Sartori AA, et al. CtIP-dependent DNA resection is required for DNA damage checkpoint maintenance but not initiation. The Journal of Cell Biology. 2012 ed. 2012;197: 869–876. doi:10.1083/jcb.201111065

50. Forment JV, Jackson SP. A flow cytometry–based method to simplify the analysis and quantification of protein association to chromatin in mammalian cells. Nat Protoc. 2015;10: 1297–1307. doi:10.1038/nprot.2015.066

51. Ferretti LP, Himmels S-F, Trenner A, Walker C, Aesch von C, Eggenschwiler A, et al. Cullin3-KLHL15 ubiquitin ligase mediates CtIP protein turnover to fine-tune DNA-

end resection. Nat Commun. 2016;7: 12628. doi:10.1038/ncomms12628

52. Stracker TH, Petrini JHJ. The MRE11 complex: starting from the ends. Nat Rev Mol Cell Biol. 2011;12: 90–103. doi:10.1038/nrm3047

53. Lim CT, Lai PJ, Leach DRF, Maki H, Furukohri A. A novel mode of nuclease action is revealed by the bacterial Mre11/Rad50 complex. Nucleic Acids Res. 2015;43: 9804–9816. doi:10.1093/nar/gkv855

54. Makharashvili N, Paull TT. CtIP: A DNA damage response protein at the intersection of DNA metabolism. DNA Repair (Amst). 2015. doi:10.1016/j.dnarep.2015.04.016

55. Katoh K, Standley DM. MAFFT Multiple Sequence Alignment Software Version 7: Improvements in Performance and Usability. Mol Biol Evol. Oxford University Press; 2013;30: 772–780. doi:10.1093/molbev/mst010

56. Söding J. Protein homology detection by HMM–HMM comparison. Bioinformatics. Oxford University Press; 2005;21: 951–960. doi:10.1093/bioinformatics/bti125

57. Guindon S, Dufayard J-F, Lefort V, Anisimova M, Hordijk W, Gascuel O. New Algorithms and Methods to Estimate Maximum-Likelihood Phylogenies: Assessing the Performance of PhyML 3.0. Syst Biol. 2010;59: 307–321. doi:10.1093/sysbio/syq010

58. Huson DH, Scornavacca C. Dendroscope 3: An Interactive Tool for Rooted Phylogenetic Trees and Networks. Syst Biol. Oxford University Press; 2012;61: 1061–1067. doi:10.1093/sysbio/sys062

59. Lupas A, Van Dyke M, Stock J. Predicting coiled coils from protein sequences. Science. 1991;252: 1162–1164. doi:10.1126/science.252.5009.1162

60. Gratias A, Bétermier M. Processing of double-strand breaks is involved in the precise excision of paramecium internal eliminated sequences. Molecular and Cellular Biology. 2003;23: 7152–7162.

61. Saudemont B, Popa A, Parmley JL, Rocher V, Blugeon C, Necsulea A, et al. The fitness cost of mis-splicing is the main determinant of alternative splicing patterns. Genome Biol. 2017;18: 208. doi:10.1186/s13059-017-1344-6

62. Galvani A, Sperling L. RNA interference by feeding in Paramecium. Trends Genet. 2002;18: 11–12.

63. Kamath RS, Martinez-Campos M, Zipperlen P, Fraser AG, Ahringer J. Effectiveness of specific RNA-mediated interference through ingested double-stranded RNA in Caenorhabditis elegans. Genome Biol. 2001;2: RESEARCH0002. doi:10.1186/gb-2000-2-1-research0002

64. Garnier O, Serrano V, Duharcourt S, Meyer E. RNA-mediated programming of developmental genome rearrangements in Paramecium tetraurelia. Molecular and Cellular Biology. 2004;24: 7370–7379. doi:10.1128/MCB.24.17.7370-7379.2004

65. Gogendeau D, Klotz C, Arnaiz O, Malinowska A, Dadlez M, de Loubresse NG, et al.

Functional diversification of centrins and cell morphological complexity. J Cell Sci. 2008;121: 65–74. doi:10.1242/jcs.019414

66. Cejka P, Kowalczykowski SC. The full-length Saccharomyces cerevisiae Sgs1 protein is a vigorous DNA helicase that preferentially unwinds holliday junctions. J Biol Chem. 2010;285: 8290–8301. doi:10.1074/jbc.M109.083196

67. Zheng L, Kanagaraj R, Mihaljevic B, Schwendener S, Sartori AA, Gerrits B, et al. MRE11 complex links RECQ5 helicase to sites of DNA damage. Nucleic Acids Res. 2009;37: 2645–2657. doi:10.1093/nar/gkp147